

Communication

On the Power of Geometry over Tetrel Bonds

Ephrath Solel  and Sebastian Kozuch * 

Department of Chemistry, Ben-Gurion University of the Negev, Beer-Sheva 841051, Israel; ephrath@post.bgu.ac.il

* Correspondence: kozuch@bgu.ac.il; Tel.: +972-8-64-61192

Received: 29 September 2018; Accepted: 23 October 2018; Published: 24 October 2018



Abstract: Tetrel bonds are noncovalent interactions formed by tetrel atoms (as σ -hole carriers) with a Lewis base. Here, we present a computational and molecular orbital study on the effect of the geometry of the substituents around the tetrel atom on the σ -hole and on the binding strengths. We show that changing the angles between substituents can dramatically increase bond strength. In addition, our findings suggest that the established Sn > Ge > Si order of binding strength can be changed in sufficiently distorted molecules due to the enhancement of the charge transfer component, making silicon the strongest tetrel donor.

Keywords: tetrel bond; σ -hole; DFT

1. Introduction

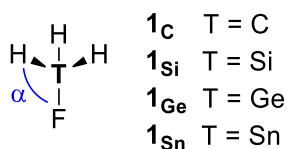
Hole interactions [1] are a relatively newly coined term that unites all noncovalent interactions in which a region of positive electrostatic potential on one atom, the hole, interacts with an electron donor. These can be based on σ , π , or δ holes depending on their type of covalent orbital origin [2]. σ -holes are formed at approximately 180° to a σ covalent bond, with the magnitude of the positive electrostatic potential depending on the electronegativity of the neighboring atoms. These interactions are further classified according to the σ -hole-bearing atom: the most studied interaction is hydrogen bonding, but there is also the widely researched halogen bonding [3–5], chalcogen bonding [6–8] (for Group VI atoms), pnictogen bonding [9–11] (Group V), tetrel bonding [12,13] (Group IV), and even aerogen bonding [14] (Group VIII). Better understanding of such noncovalent interactions can help in the study and future design of novel supramolecular complexes, catalysts, and crystal engineering.

Herein, we focus on the effect that the angles around the atom have on the binding strengths of tetrel bonds. We analyze this by examining the effect on the electrostatic hole and on the frontier orbitals in order to explain the dramatic changes in complexation energies. These effects were previously observed in a survey of the Cambridge Structural Database [12]: carbon demonstrates almost nonexistent σ -holes relative to Si, Ge, and Sn [13], with the only found crystal structures exhibiting σ -hole interactions with C based on three-membered rings [15] or cubanes [16], in which the angles around the carbon are far from the optimal tetrahedral angle. The effect of the angles between covalent bonds on interaction strength was also computationally explained by showing that smaller rings cause the σ -hole to be more exposed, increasing its electrostatic potential [12].

It should be noted that upon binding with a Lewis base, there is geometrical deformation around the tetrel atom as substituents move to make more room for the electron donor [17], a distortion that was computed to be more energetically costly for smaller atoms. Freezing the monomer in the complex's distorted geometry eliminates the deformation energy and results in an increase in the tetrel interaction energy. Our aim in this study is to understand the effect of the molecular geometry on bond energy beyond such binding-caused distortions by applying molecular orbital theory on the bonding patterns.

2. Results and Discussion

To estimate the effect the substituent angles have on the σ -hole and on the shape of the frontier orbitals, we examined the TH_3F systems ($\mathbf{1}_T$, with $T = \text{C, Si, Ge, and Sn}$, Scheme 1). A weak σ -hole may be formed at the extension of the T-H bonds, but evidently the σ -hole corresponding to the T-F bond is the dominant one. We considered the optimized structures (C_{3V}) with no constraints or at three different fixed F-T-H angles ($\alpha = 109^\circ, 100^\circ, \text{ and } 90^\circ$). All computations were performed at the MN15/Def2-TZVPD [18,19] level of theory with Gaussian16 [20] (see the Methods section).



Scheme 1. $\mathbf{1}_T$ model systems.

As can be seen in Figure 1, the LUMO for $\mathbf{1}_C$ is an antibonding F-C σ^* . This orbital mostly resides at the extension of the F-T bond (as in all $\mathbf{1}_T$ molecules, see Figures S1–S3) and forms interactions with Lewis bases by charge transfer. For all $\mathbf{1}_T$ molecules, the LUMO shows a larger lobe at the extension of the T-F bond as the angle decreases, which, in principle, aids the orbital interaction with the nucleophile.

The $\sigma_{\text{F-T}}$ orbitals (typically, the HOMO-2) are expected to match the areas with higher and lower electron density [2,21]. In $\mathbf{1}_C$, the electrostatic hole did not match this criterion. At smaller α , the outer lobe on C was slightly larger, although the electrostatic potential was more positive (Figure 1 and Table 1). For $\mathbf{1}_{\text{Si}}$, $\mathbf{1}_{\text{Ge}}$, and $\mathbf{1}_{\text{Sn}}$, due to the larger and more electropositive tetrel atom, the $\sigma_{\text{F-T}}$ was more localized on the F and more affected by the hydrogens. Thus, there was somewhat less electron density at the outer lobe of $\sigma_{\text{F-T}}$ at smaller angles, which, in principle, matches the trend in the $V_{s,\text{max}}$ (the maximum positive potential on the electrostatic potential (ESP) isosurface; see Figure 1 and Table 1). However, it seems that the HOMOs ($\sigma_{\text{H-T}}$ orbitals) are the ones mostly responsible of taking out the electron density, enhancing the σ -hole as the angle decreases by moving the T-H away from the F-T axis (matching the $V_{s,\text{max}}$ trend—see Table 1—and the ESP maps—Figure 1 and Figures S1–S3).

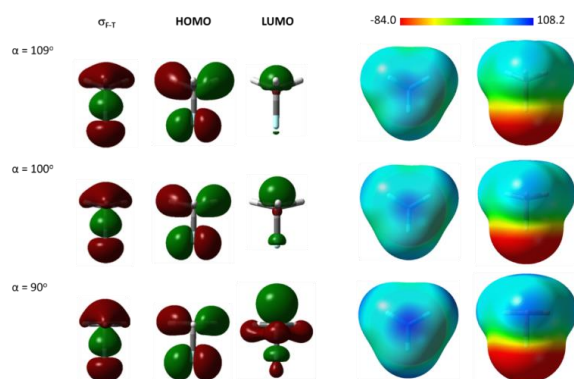


Figure 1. Chosen MOs and electrostatic potential (ESP) maps for $\mathbf{1}_C$ with three different F-C-H angles (α). ESP maps are on the 0.001 density isosurface. The color scale is in kJ mol^{-1} . $\sigma_{\text{F-T}}$ corresponds to the bonding F-T σ orbital, irrespective of its position compared to other orbitals. The HOMO is doubly degenerate.

As can be expected, the F-T-H angle modifies the degree of sp hybridization of different orbitals. In NH_3 [22], the frontier MOs of the planar geometry exhibit pure s or p orbitals on the nitrogen, which then mix as the angle of pyramidalization increases. Similarly, according to the NBO analysis in $\mathbf{1}_T$, the tetrel component of the $\sigma_{\text{F-T}}$ MO has a higher p character when the angle is 90° , which decreases when the α angle increases (opposite to the s character; see Table 1). This causes stronger $\sigma_{\text{F-T}}$ (shorter F-T

bond length) with larger α by focalizing the lobe into the fluorine's direction (Table 1), while also marginally reducing the outer lobe in 1_C , as explained above (Figure 1).

Table 1. Properties of 1_T with different σ angles: σ_{F-T} and LUMO energies (kJ mol^{-1}), F-T bond length (\AA), %s and %p on T in the NBO F-T σ bond, and the maximal positive electrostatic potential at the σ hole (kJ mol^{-1}).

T	α	σ_{F-T}	LUMO	d_{F-T}	%s ^b	%p ^b	$V_{s,max}$
C	Opt. (109.1°) ^a	−1413.9	154.7	1.376	21.52	78.28	81.2
	109°	−1413.2	154.7	1.376	21.48	78.32	81.2
	100°	−1328.6	147.6	1.426	16.09	83.71	84.1
	90°	−1232.6	84.6	1.511	8.53	91.25	95.2
Si	Opt. (108.3°) ^a	−1328.8	27.2	1.598	21.40	76.03	142.5
	109°	−1332.2	28.7	1.596	21.62	75.81	137.3
	100°	−1282.5	−22.8	1.617	18.39	78.95	200.6
	90°	−1212.8	−123.7	1.655	13.54	83.79	256.5
Ge	Opt. (106.2°) ^a	−1250.8	19.4	1.737	19.96	79.06	164.5
	109°	−1267.7	21.4	1.731	21.20	77.83	148.8
	100°	−1212.4	−18.6	1.751	17.05	81.98	197.0
	90°	−1145.6	−120.0	1.788	11.39	87.66	238.0
Sn	Opt. (104.4°) ^a	−1158.6	−32.6	1.927	18.66	80.49	196.6
	109°	−1182.5	−46.3	1.920	20.75	78.41	170.9
	100°	−1134.9	−58.2	1.935	16.56	82.57	218.6
	90°	−1079.2	−158.9	1.962	11.20	87.94	255.7

^a Fully optimized molecule, with no angle restrictions. ^b %s and %p are the same for both the bonding and antibonding orbitals.

We computed the complexes of 1_T with HCN, a prototypical Lewis base for hole interactions that minimizes the influences coming from atoms and bonds other than the tetrel bond (ammonia, for example, exhibits attraction between its partially positive hydrogens and the partially negative hydrogens on the tetrrels). The geometry parameters, dissociation energies ($D_e = E_{1_T} + E_{HCN} - E_{1_T \cdots NCH}$), and NBO charge transfer energies (i.e., the $n \rightarrow \sigma^*$ perturbational stabilization energy, E^2) are presented in Table 2.

Table 2. Properties of the complexes of 1_T with HCN at different α angles: (distances in \AA , energies in kJ mol^{-1}).

T	α	d_{T-F}	$d_{T \cdots N}$	% Cov. Rad. ^b	D_e ^c	$E^2_{n \rightarrow \sigma^*}$ ^d
C	Opt. (109.3°) ^a	1.380	3.154	208	9.3	2.5
	109°	1.381	3.155	208	9.2	2.5
	100°	1.432	3.116	205	8.7	3.0
	90°	1.521	3.013	198	9.5	5.3
Si	Opt. (106.3°) ^a	1.608	2.847	153	18.7	18.0
	109°	1.602	2.944	158	17.0	13.6
	100°	1.625	2.576	138	29.8	37.7
	90°	1.670	2.162	116	56.7	84.1 ^e
Ge	Opt. (104.6°) ^a	1.749	2.931	149	20.4	24.6
	109°	1.738	3.043	154	17.8	18.4
	100°	1.763	2.804	142	25.4	33.9
	90°	1.808	2.532	128	37.8	68.1
Sn	Opt. (102.2°) ^a	1.945	2.934	136	25.7	27.0
	109°	1.930	3.086	143	20.8	17.4
	100°	1.950	2.887	134	28.9	31.0
	90°	1.982	2.703	125	39.4	54.3

^a Fully optimized molecule with no angle restrictions. ^b Ratio between tetrel bond and the sum of covalent radii of T and N. ^c Tetrel bond dissociation energies. ^d Perturbational stabilization energy according to NBO analysis corresponding to charge transfer. ^e $E^2_{n \rightarrow \sigma^*}$ for this complex was calculated by extrapolation, see Supplementary Information.

Table 2 shows that the T-F bonds are all longer compared to the free molecules, as expected upon interaction of a Lewis base with the σ^* orbital. Bond strength, due to the higher polarizabilities of the heavier tetrel atoms, is $1_{\text{C}} \ll 1_{\text{Si}} < 1_{\text{Ge}} < 1_{\text{Sn}}$ for the fully optimized molecules or for $\alpha = 109^\circ$. For the smaller α angles, the T...N distance is shorter and the binding energies larger compared to the unconstrained systems (except for 1_{C} , which at any rate exhibits very weak binding), with the largest changes with respect to the angle observed with 1_{Si} (see Figure 2A). If we check the effect of changing the tetrel atom at each fixed α angle (Figure 2B), we can see that Ge and Sn show stronger binding than Si only for the fully optimized geometry and for $\alpha = 109^\circ$. However, upon reduction of the angle to 100° and 90° , the Si shows higher binding than the other tetrel atoms, with significantly shorter T...N distances. As can be seen in Table 2, for $\alpha = 90^\circ$ the T...N distances for 1_{Si} , 1_{Ge} , and 1_{Sn} come close to the sum of the covalent radii of T and nitrogen, pointing to a more covalent character (in the extreme case of 1_{Si} , bond length is only 116% compared to the sum of the covalent radii). In addition, the NBO $n \rightarrow \sigma^*$ component grows as $\text{Si} > \text{Ge} > \text{Sn}$ for the smaller α angles (Figure 2C). This suggests that there are two competing factors affecting binding strength: polarizability, which increases upon descending the column, increasing electrostatic interactions; and orbital interactions, which are stronger for smaller atoms, except for C, and become more dominant at shorter distances and smaller α angles.

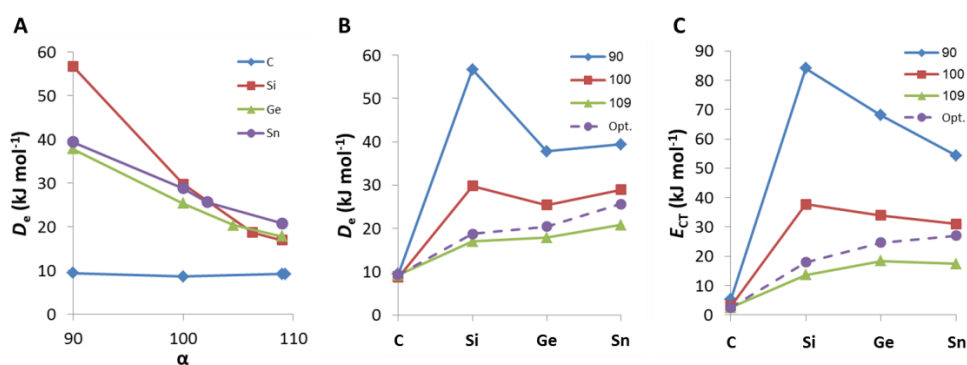


Figure 2. Complexation of 1_{T} with HCN: (A) dissociation energy as a function of the α angle; (B) dissociation energy as a function of the tetrel atom; (C) NBO $n \rightarrow \sigma^*$ charge transfer energy as a function of the tetrel atom.

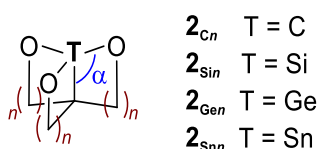
We plotted the dissociation energy of the $1_{\text{T}} \cdots \text{NCH}$ complexes as a function of both the NBO $n \rightarrow \sigma^*$ charge transfer energy and the $V_{\text{s,max}}$ of the uncomplexed tetrel molecules (see Figure S4), which correlate, respectively, with the orbital and electrostatic interactions. The graphs show a linear relationship, indicating that the charge transfer component and the electrostatic interaction (connected with the virtual and occupied MOs of the hole bearer, respectively) go hand in hand in hole interactions [2,21]. However, there is one clear outlier in the $V_{\text{s,max}}$ graph (Figure S4B) corresponding to 1_{Si} at 90° , for which the electrostatic potential is an insufficient descriptor. This would suggest that, for complexes with stronger binding energies and smaller intermolecular distances, orbital interaction is more significant—a sign of an incipient covalent bond.

Our results clearly show that at small angles there is a departure from the expected binding order of $\text{Sn} > \text{Ge} > \text{Si} > \text{C}$, as the 1_{Si} shows strongest binding for angles of 100° and 90° . This comes as a result of the better interaction between silicon and nitrogen orbitals compared to the larger Ge and Sn. However, an alternative way to look at this is to check the energy needed to distort the molecules before and after complexation [11]. For $\alpha = 100^\circ$ and 90° , the distortion energy of the monomer is almost always larger than for the complex (Table S1). The difference in distortion energies (ΔE_{dist}) is particularly large for Si (38 kJ mol^{-1} at $\alpha = 90^\circ$). As the difference in distortion energies equals the difference in dissociation energies ($\Delta E_{\text{dist}} = D_e \text{ constrained} - D_e \text{ optimized}$), this can also explain the dramatic increase of complexation energy for 1_{Si} at these angles.

So far, previous observations suggest that the geometry around the tetrel atom can have significant influence on the strength of the tetrel bonds, leading to unusually strong bonds at small angles,

especially for T = Si. In order to check this trend in more realistic molecular models, we studied the 2_{Tn} molecules (Scheme 2, with a C_3 symmetry). Here, each α angle depends on the varying size of the rings determined by the number of carbon links (n). In 2_{Tn} , the σ -hole is at the extension of the T-C bond and not of the T-O bonds, but the magnitude of the central hole is enlarged by the oxygens (with methylenes instead of oxygens, the σ -hole was smaller and similar in magnitude to the holes on the methylene hydrogens). Many alkoxyasilanes and alkoxygermanes are known, and there is also an experimental example similar to 2_{Si2} in which the Si forms strong interactions with electron donors [23].

As can be seen from Table 3, 2_{Cn} does not show binding when $n = 2$ or 3, and only a decrease in the C-C-O angle to 97° ($n = 1$) produces some very weak binding. For heavier tetrels, as the number of links (and, correspondingly, α) decreases, the dissociation energy shows significant increase. For $n = 3$ (close to the unconstrained angles), the dissociation energy has the expected $Sn > Ge > Si$ order. Si and Ge show very similar binding energies for the different n 's, with an unfavorable binding for $n = 3$, but strong binding for $n = 1$ ($D_e > 100$ kJ mol $^{-1}$). The difference in dissociation energies between 2_{Si1} and 2_{Ge1} is negligible, but α is smaller for Ge. This points at the same trend we saw for 1_T —the most dramatic increase in binding with smaller angles occurs with silicon (Figure S5). However, this does not actually make 2_{Si1} the stronger binder due to the smaller α in 2_{Ge1} (if both species had the same α angles, then 2_{Si1} would probably have the higher D_e).



Scheme 2. 2_{Tn} systems.

Table 3. Bond distances, angles, dissociation energies, and $V_{s,max}$ of 2_{Tn} , and their binding complexes with HCN (distances in Å, energies in kJ mol $^{-1}$).

T	n	d_{T-C} Monomer	d_{T-C} Complex	α Monomer	α Complex	$d_{T...N}$	% Cov. Rad. ^c	D_e	$V_{s,max}$ ^d
C	1	1.481	1.486	97.6	97.1	2.953	194.3	0.9	42.1
	2	1.561	-	107.8	-	-	-	NB	-107.2
	3	1.542	-	111.4	-	-	-	NB	-153.5
Si	1	1.884	1.954	88.7	83.8	1.931	103.8	111.3	260.3
	2	1.830	1.879	101.0	95.6	2.084	112.0	42.3	147.6
	3 ^a	1.854	1.860	108.5	107.7	3.549	190.8	-3.2	-28.7
Ge	1	1.974	2.043	83.2	79.8	2.047	103.9	112.6	339.2
	2	1.899	1.935	98.9	95.4	2.220	112.7	47.9	186.6
	3	1.934	1.944	109.4	107.8	3.198	162.3	-1.2	9.8
Sn ^b	2	2.077	2.104	93.0	91.0	2.318	107.3	73.9	264.5
	3	2.118	2.147	107.9	104.1	2.470	114.4	30.3	140.2

^a The complex with HCN interacting with the σ -hole is actually a maximum in energy as attraction between the oxygens and the positive charge of HCN are significant. ^b 2_{Sn1} is unstable. ^c Ratio of the tetrel bond and the sum of covalent radii of T and N. ^d Measured at the extension of the C-T bond.

3. Conclusions

Besides the classical enhancement of the tetrel bond brought by having heavier tetrels, geometry can be an important factor in bond strength. In addition to the release of strain energy [17], a smaller angle between the substituents not only favors the bond by geometrically exposing the tetrel atom, but there is also an electronic effect that boosts the σ -hole and aids the charge transfer. These effects cannot appear in regular halogen bonding due to a lack of side substituents, but can be a feature in pnictogen and chalcogen bonds, or in hypercoordinated halogens [21]. Our findings suggest that, in designing new tetrel bonded complexes, focusing on the geometry around the tetrel atom could

allow the use of the more abundant silicone compared to the heavier elements without significantly sacrificing binding strength.

4. Methods

All density functional theory (DFT) computations were done at the MN15/Def2-TZVPD [18,24] level with Gaussian16 [20]. All energies reported do not include ZPE correction. All minima were confirmed with frequency computations. In order to check the validity of the used DFT method, the dissociation energies for $\mathbf{1}_{\text{Si}}$ and $\mathbf{1}_{\text{Ge}}$ were computed with CCSD(T)/CBS (complete basis set extrapolation from aug-cc-pvtz/aug-cc-pvqz, carried out in ORCA [25]) at the geometries found by MN15/Def2-TZVPD (see Table S2). The CCSD(T)/CBS results showed values very close to those of DFT, with a maximum difference of 8.2 kJ mol⁻¹, and displayed the same trends (stronger binding for $\mathbf{1}_{\text{Ge}}$ at 109° and for $\mathbf{1}_{\text{Si}}$ at 90°). NBO analyses were done with NBO3.1 [26] as appears in Gaussian16.

Supplementary Materials: The following are available online: Figures S1–S3: Chosen MOs and ESP maps for $\mathbf{1}_{\text{C}}$, $\mathbf{1}_{\text{Ge}}$, $\mathbf{1}_{\text{Sn}}$ with three different F-T-H angles; Figure S4: graphs for the complexation of $\mathbf{1}_{\text{T}}$ with HCN; Figure S5: graphs for the complexation of $\mathbf{2}_{\text{Tn}}$ with HCN.

Author Contributions: E.S. and S.K. both contributed to the conceptualization, computation and writing of this project.

Funding: This research was funded by the Israeli Science Foundation (grant No. 631/15) and the German–Israeli Foundation (grant I-2481-302.5/2017). E.S. acknowledges funding from the Israeli Ministry of Science and Technology through the Shulamit Aloni Fellowship for Promoting Women in Science, and from the Kreitman Foundation Postdoctoral Fellowship.

Conflicts of Interest: The authors declare no conflict of interest. The funders had no role in the design of the study; in the collection, analyses, or interpretation of the data; in the writing of the manuscript; and in the decision to publish the results.

References

1. Clark, T.; Hennemann, M.; Murray, J.S.; Politzer, P. Halogen bonding: The σ -hole. *J. Mol. Model.* **2007**, *13*, 291–296. [[CrossRef](#)] [[PubMed](#)]
2. Angarov, V.; Kozuch, S. On the σ , π and δ hole interactions: A molecular orbital overview. *New J. Chem.* **2018**, *42*, 1413–1422. [[CrossRef](#)]
3. Politzer, P.; Lane, P.; Concha, M.C.; Ma, Y.; Murray, J.S. An overview of halogen bonding. *J. Mol. Model.* **2007**, *13*, 305–311. [[CrossRef](#)] [[PubMed](#)]
4. Politzer, P.; Murray, J.S.; Clark, T. Halogen bonding and other σ -hole interactions: A perspective. *Phys. Chem. Chem. Phys.* **2013**, *15*, 11178–11189. [[CrossRef](#)] [[PubMed](#)]
5. Auffinger, P.; Hays, F.A.; Westhof, E.; Ho, P.S. Halogen bonds in biological molecules. *Proc. Natl. Acad. Sci. USA* **2004**, *101*, 16789–16794. [[CrossRef](#)] [[PubMed](#)]
6. Wang, W.; Ji, B.; Zhang, Y. Chalcogen bond: A sister noncovalent bond to halogen bond. *J. Phys. Chem. A* **2009**, *113*, 8132–8135. [[CrossRef](#)] [[PubMed](#)]
7. Mahmudov, K.T.; Kopylovich, M.N.; Guedes da Silva, M.F.C.; Pombeiro, A.J.L. Chalcogen bonding in synthesis, catalysis and design of materials. *Dalton Trans.* **2017**, *46*, 10121–10138. [[CrossRef](#)] [[PubMed](#)]
8. Pascoe, D.J.; Ling, K.B.; Cockroft, S.L. The origin of chalcogen-bonding interactions. *J. Am. Chem. Soc.* **2017**, *139*, 15160–15167. [[CrossRef](#)] [[PubMed](#)]
9. Scheiner, S. A new noncovalent force: Comparison of P...N interaction with hydrogen and halogen bonds. *J. Chem. Phys.* **2011**, *134*, 094315. [[CrossRef](#)] [[PubMed](#)]
10. Del Bene, J.E.; Alkorta, I.; Elguero, J. The pnictogen bond in review: Structures, binding energies, bonding properties, and spin-spin coupling constants of complexes stabilized by pnictogen bonds. In *Noncovalent Forces*; Scheiner, S., Ed.; Springer International Publishing: New York, NY, USA, 2015.
11. Adhikari, U.; Scheiner, S. Comparison of P...D (D = P,N) with other noncovalent bonds in molecular aggregates. *J. Chem. Phys.* **2011**, *135*, 184306. [[CrossRef](#)] [[PubMed](#)]
12. Bauzá, A.; Mooibroek, T.J.; Frontera, A. Tetrel bonding interactions. *Chem. Rec.* **2016**, *16*, 473–487. [[CrossRef](#)] [[PubMed](#)]

13. Murray, J.S.; Lane, P.; Politzer, P. Expansion of the σ -hole concept. *J. Mol. Model.* **2009**, *15*, 723–729. [[CrossRef](#)] [[PubMed](#)]
14. Bauzá, A.; Frontera, A. Aerogen bonding interaction: A new supramolecular force? *Angew. Chem. Int. Ed.* **2015**, *54*, 7340–7343. [[CrossRef](#)]
15. Anisimov, V.M.; Zolotoi, A.B.; Antipin, M.Y.; Lukin, P.M.; Nasakin, O.E.; Struchkov, Y.T. Hexacyanocyclopropane. Synthesis and structure. *Mendeleev Commun.* **1992**, *2*, 24–25. [[CrossRef](#)]
16. Bauzá, A.; Mooibroek, T.J.; Frontera, A. Influence of ring size on the strength of carbon bonding complexes between anions and perfluorocycloalkanes. *Phys. Chem. Chem. Phys.* **2014**, *16*, 19192–19197. [[CrossRef](#)] [[PubMed](#)]
17. Zierkiewicz, W.; Michalczyk, M.; Scheiner, S. Implications of monomer deformation for tetrel and pnictogen bonds. *Phys. Chem. Chem. Phys.* **2018**, *20*, 8832–8841. [[CrossRef](#)] [[PubMed](#)]
18. Yu, H.S.; He, X.; Li, S.L.; Truhlar, D.G. MN15: A Kohn–Sham global-hybrid exchange–correlation density functional with broad accuracy for multi-reference and single-reference systems and noncovalent interactions. *Chem. Sci.* **2016**, *7*, 5032–5051. [[CrossRef](#)] [[PubMed](#)]
19. Kozuch, S.; Martin, J.M.L. Halogen bonds: Benchmarks and theoretical analysis. *J. Chem. Theory Comput.* **2013**, *9*, 1918–1931. [[CrossRef](#)] [[PubMed](#)]
20. Frisch, M.J.; Trucks, G.W.; Schlegel, H.B.; Scuseria, G.E.; Robb, M.A.; Cheeseman, J.R.; Scalmani, G.; Barone, V.; Petersson, G.A.; Nakatsuji, H.; et al. *Gaussian 16 (Revision A.03)*; Gaussian, Inc.: Wallingford, UK, 2016.
21. Kirshenboim, O.; Kozuch, S. How to twist, split and warp a σ -hole with hypervalent halogens. *J. Phys. Chem. A* **2016**, *120*, 9431–9445. [[CrossRef](#)] [[PubMed](#)]
22. Walsh, A.D. 469. The electronic orbitals, shapes, and spectra of polyatomic molecules. Part IV. Tetratomic hydride molecules, AH₃. *J. Chem. Soc. (Resumed)* **1953**, 2296–2301. [[CrossRef](#)]
23. Kobayashi, J.; Kawaguchi, K.; Kawashima, T. Water-coordinated neutral silane complex: A frozen intermediate of hydrolysis of alkoxy silanes. *J. Am. Chem. Soc.* **2004**, *126*, 16318–16319. [[CrossRef](#)] [[PubMed](#)]
24. Rappoport, D.; Furche, F. Property-optimized Gaussian basis sets for molecular response calculations. *J. Chem. Phys.* **2010**, *133*, 134105. [[CrossRef](#)] [[PubMed](#)]
25. Neese, F. The ORCA program system. *Wiley Interdiscip. Rev. Comput. Mol. Sci.* **2012**, *2*, 73–78. [[CrossRef](#)]
26. Glendening, E.D.; Reed, A.E.; Carpenter, J.E.; Weinhold, F. *NBO*, Version 3.1; TCI: Madison, WI, USA, 1998.

Sample Availability: Samples of the compounds are not available from the authors.



© 2018 by the authors. Licensee MDPI, Basel, Switzerland. This article is an open access article distributed under the terms and conditions of the Creative Commons Attribution (CC BY) license (<http://creativecommons.org/licenses/by/4.0/>).